Physics of non-adiabatic transport and field-domain effect in quantum-well infrared photodetectors

Danhong Huang [*], D.A. Cardimona

Air Force Research Laboratory, VSSS, 3550 Aberdeen Ave SE, Kirtland AFB, NM 87117, USA

Abstract

A previous theory for studying the distribution of non-uniform fields in multiple-quantum-well photodetectors under an ac voltage is generalized by including non-adiabatic space-charge-field effects. Numerical calculations indicate that field-domain effects are only important at high temperatures or high voltages when both injection and sequential-tunneling currents are significant. On the other hand, it is found that the non-adiabatic effects included in this generalized theory become significant at low temperatures and low voltages when field-domain effects are negligible. In order to explain the non-adiabatic charge-density fluctuations quantum-statistically, a non-adiabatic differential equation is derived based on the self-consistent Hartree model by using a shifted Fermi–Dirac model for the local fluctuation of electron distributions. The non-adiabatic effect is found to cause an "equilibrium" state variation with time under an ac voltage.
© 2003 Elsevier B.V. All rights reserved.

PACS: 73.40.−c; 73.40.Gk; 73.40.Kp; 73.21.Fg

Keywords: Non-adiabatic; Domain; Hartree; Distribution; Tunneling; Quantum-well

1. Introduction

Multiple-quantum-well (MQW) photodetectors using intersubband transitions have attracted a lot of studies over the past few years [1]. Transient spectroscopy allows us to gain information on the sequential-tunneling processes between quantum wells (QWs) and thus QW parameters, including geometric and QW capacitances at the same time.

Recently, a residual dark current in quantum-well infrared photodetectors (QWIPs) was reported when an ac bias voltage was swept through zero [2]. Later, a roll-off of the dynamical responsivity in QWIPs was observed when the frequency of a chopped incident optical flux was increased beyond a certain value [3]. More recently, a counterclockwise hysteresis loop for the tunneling current and a clockwise hysteresis loop for the emission current in QWIPs was seen experimentally as the device temperature was swept up from 10 to 300 K and then back down [4]. These new phenomena found in QWIPs were physically explained by a non-adiabatic sequential-tunneling model [5]. The non-adiabatic effect discussed in this paper refers

---
[*] Corresponding author. Tel.: +1-505-846-5788; fax: +1-505-846-6098.

E-mail address: danhong.huang@kirtland.af.mil (D. Huang).

Report Documentation Page

1. REPORT DATE **2003**	2. REPORT TYPE	3. DATES COVERED **-**

4. TITLE AND SUBTITLE	5a. CONTRACT NUMBER
Physics of non-adiabatic transport and field-domain effect in quantum-well infrared photodetectors	5b. GRANT NUMBER
	5c. PROGRAM ELEMENT NUMBER
6. AUTHOR(S) **Danhong Huang; D Cardimona**	5d. PROJECT NUMBER
	5e. TASK NUMBER
	5f. WORK UNIT NUMBER

7. PERFORMING ORGANIZATION NAME(S) AND ADDRESS(ES) **Air Force Research Laboratory/VSSS,3550 Aberdeen Ave SE,Kirtland AFB,NM,87117-5776**	8. PERFORMING ORGANIZATION REPORT NUMBER

9. SPONSORING/MONITORING AGENCY NAME(S) AND ADDRESS(ES)	10. SPONSOR/MONITOR'S ACRONYM(S)
	11. SPONSOR/MONITOR'S REPORT NUMBER(S)

12. DISTRIBUTION/AVAILABILITY STATEMENT
Approved for public release; distribution unlimited

13. SUPPLEMENTARY NOTES

14. ABSTRACT
A previous theory for studying the distribution of non-uniform fields in multiple-quantum-well photodetectors under an ac voltage is generalized by including non-adiabatic space-charge-field effects. Numerical calculations indicate that field-domain effects are only important at high temperatures or high voltages when both injection and sequential-tunneling currents are significant. On the other hand, it is found that the non-adiabatic effects included in this generalized theory become significant at low temperatures and low voltages when field-domain effects are negligible. In order to explain the non-adiabatic charge-density fluctuations quantum-statistically, a non-adiabatic differential equation is derived based on the self-consistent Hartree model by using a shifted Fermi-Dirac model for the local fluctuation of electron distributions. The non-adiabatic effect is found to cause an "equilibrium" state variation with time under an ac voltage.

15. SUBJECT TERMS

16. SECURITY CLASSIFICATION OF:			17. LIMITATION OF ABSTRACT	18. NUMBER OF PAGES	19a. NAME OF RESPONSIBLE PERSON
a. REPORT **unclassified**	b. ABSTRACT **unclassified**	c. THIS PAGE **unclassified**		**16**	

to the fact that a transient current not only depends on the magnitude of an electric field, but also depends on its time derivative.

For the field-domain effect, we generalize the previous theory [6] for studying the distribution of non-uniform fields in MQW photodetectors under an ac voltage by including non-adiabatic space-charge-field effects. We find from numerical results that field-domain effects are only important at high temperatures or high voltages when both injection and sequential-tunneling currents are significant. On the other hand, we find that non-adiabatic effects included in the generalized theory become visible at low temperatures and low voltages when field-domain effects are negligible. The time duration for non-adiabatic effects is found to depend on the quantum capacitance, while the classical dielectric displacement current is found to be related to the geometric capacitance. Moreover, a negative conduction current is predicted under a positive voltage in non-steady state.

For non-adiabatic transport, we consider electrons in a MQW system in the presence of a uniform ac electric field. We assume that electrons during the sequential-tunneling process only see an instantaneous electric field and stay in equilibrium states due to very fast elastic and inelastic scattering inside the quantum well. The non-adiabatic effect causes an ''equilibrium'' state to vary with time. As a result, the charge-density fluctuation in the QW will modify the Hartree potential in the surrounding barrier region, and thus greatly affect the sequential tunneling of electrons through the barrier. Simultaneously, the non-adiabatic fluctuation of charge density also modifies electronic states in the quantum well within the self-consistent Hartree model [7].

The organization of the paper is as follows. In Section 2, we introduce our model for classical charge-density fluctuations and the distribution of field domains in MQWs. In Section 3, we generalize the model to include quantum non-adiabatic charge-density fluctuations and their effects on the distribution of field domains in MQWs. Section 4 is devoted to the derivation of a non-adiabatic differential equation based on the self-consistent Hartree model by using a shifted Fermi–Dirac model for the local fluctuation of electron distributions and provides a quantum-statistical explanation for the non-adiabatic charge-density fluctuations introduced in Section 2. Some numerical results for classical and quantum charge fluctuations, as well as for non-adiabatic fluctuations in electron distributions, are presented in Section 5. The paper is concluded in Section 6.

2. Classical charge fluctuations

In this section, we study effects of field domains resulting from the imbalance between injection and sequential-tunneling currents and show that these effects become negligible at low temperatures and voltages.

Electrons in QWs are confined in the direction perpendicular to the wells, while electrons in heavily-doped contact layers are free in all three directions. Therefore, we expect the tunneling of electrons from a contact layer to a QW (3D-to-2D) will be physically different than that from one QW to another (2D-to-2D).

As shown in Fig. 1, we see that the distribution of uniform dc electric fields in (a) with $\mathscr{E}_0 = \mathscr{E}_1 = \mathscr{E}_2 = \cdots = \mathscr{E}_N$ is not stable if the injection current flowing from the left contact layer to the first QW and the sequential-tunneling current flowing from the first QW to the second QW are different [6,8,9]. As an example, we assume in (b) that the injection current is smaller than the sequential-tunneling current. In this situation, the local field $\mathscr{E}_0$ in the first (emitter) barrier layer has to be increased so as to equalize these two currents. As a result of $\mathscr{E}_0 > \mathscr{E}_1 = \mathscr{E}_2 = \cdots = \mathscr{E}_N$, we know from the Maxwell equations that the charge density in the first QW will be reduced relative to the others [8], i.e. $\rho_1 < \rho_2 = \rho_3 = \cdots = \rho_N$. Now, let us further compare the tunneling currents flowing from the first QW to the second QW and that flowing from the second QW to the third QW. We realize from (c) that the tunneling current flowing from the first QW is less than that flowing from the second QW since $\rho_1 < \rho_2$ for $\mathscr{E}_1 = \mathscr{E}_2$. Therefore, $\mathscr{E}_1 > \mathscr{E}_2 = \cdots = \mathscr{E}_N$ is required so as to equalize these two sequential-tunneling currents.
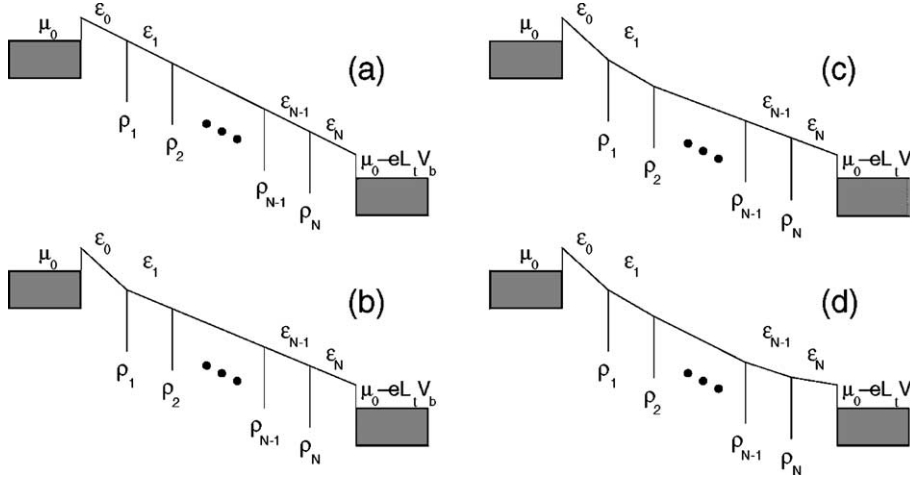
Fig. 1. The processes (a)–(d) for the formation of field domains in a multiple-quantum-well (MQW) sample with N quantum wells (QWs). Here, $\mathscr{E}_k$ for $k = 0, 1, 2, \ldots, N$ indicates local electric fields in $(N + 1)$ different barrier layers, and ρ_k for $k = 1, 2, \ldots, N$ corresponds to different charge densities inside N QWs. μ_0 is the chemical potential in contact layers, V_b is the applied voltage, and L_t is the total length of MQWs.

Consequently, we are left with $\rho_1 < \rho_2 < \rho_3 = \cdots = \rho_N$. This process will continue up to the last (Nth) QW, as displayed in (d), until the initial field distribution $\mathscr{E}_0 > \mathscr{E}_1 > \mathscr{E}_2 > \cdots > \mathscr{E}_N$ and density distribution $\rho_1 < \rho_2 < \rho_3 < \cdots < \rho_N$ are reached. Here, the local field $\mathscr{E}_j$ is a constant in the jth barrier layer, and the splitting of different local electric fields constructs the field domains in MQWs. The electric fields in different barrier regions in steady state will be redistributed if the total tunneling current flowing into the bottom contact layer is different from the injection current flowing out of the top contact layer. Therefore, the above field-adjustment process will be repeated again and again until the total tunneling current flowing to the bottom contact layer is equal to the injection current flowing from the top contact layer, and then, a stable distribution of local fields is formed. It should be noted that the distribution of electric-field domains in steady state depends on the value of voltage applied at each moment. A variation of the applied voltage with time results in charge-density oscillations in each QW, and varying field domains as well.

The injection current density (3D-to-2D) from the top contact layer to the first QW is calculated to be [8]

$$
J_{\mathrm{inj}}^{\mathrm{3D}}[\mu_0, \mu_1(t), \mathscr{E}_0(t)]
$$

$$
= \frac{e m^* k_{\mathrm{B}} T}{2\pi^2 \hbar^3} \frac{\mathscr{E}_0(t)}{|\mathscr{E}_0(t)|} \int_0^{+\infty} \mathrm{d}E \, \mathscr{T}[E, |\mathscr{E}_0(t)|]
$$

$$
\times \ln\left\{ \frac{1 + \exp\left[(\mu_0 - E)/k_{\mathrm{B}} T\right]}{1 + \exp\left[(\mu_1(t) - E - e L_{\mathrm{B}}|\mathscr{E}_0(t)|)/k_{\mathrm{B}} T\right]} \right\},
$$

(1)

where t is the time, m^* is the effective mass of electrons, T is the electron (or lattice) temperature, L_{B} is the thickness of the barrier, $\mathscr{T}[E, |\mathscr{E}(t)|]$ is the quantum transmission of electrons [10] with kinetic energy E through a barrier biased by an electric field $\mathscr{E}(t)$, and the chemical potential μ_0 in the contact layer is related to the electron concentration n_{c} by

$$
n_{\mathrm{c}} = \frac{1}{2\pi^2}\left(\frac{2m^*}{\hbar^2}\right)^{3/2} \int_0^{+\infty} \mathrm{d}E \sqrt{E}\left[1 + \exp\left(\frac{E - \mu_0}{k_{\mathrm{B}} T}\right)\right]^{-1}.
$$

For low T, electrons in QWs can only populate the ground subband with quantized energy E_0. Furthermore, the sequential-tunneling current density (2D-to-2D) from the kth QW to the neighboring $(k + 1)$th QW is found to be [1]

$$J_k^{2D}[\mu_k(t), \mu_{k+1}(t), \mathscr{E}_k(t)]$$

$$= \frac{em^*}{\pi\hbar^2 L_W} v_k^d[\mathscr{E}_k(t)] \int_0^{+\infty} dE\, \mathscr{T}[E + E_0, |\mathscr{E}_k(t)|]$$

$$\times \left\{ f_0[E - \mu_k(t)] - f_0[E - \mu_{k+1}(t) + eL_B|\mathscr{E}_k(t)|] \right\}, \tag{2}$$

where L_W is the well width, $k = 1, 2, \ldots, N$ represents the index of N wells, $k = N + 1$ corresponds to the bottom contact layer, $\mu_{N+1} = \mu_0$, $f_0(x) = [1 + \exp(x/k_B T)]^{-1}$, and the chemical potential $\mu_k(t)$ in the kth QW introduced in Eqs. (1) and (2) can be determined by the electron density $n_k(t)$ in the kth QW through

$$\mu_k(t) = k_B T \ln \left\{ \exp\left[\frac{\pi\hbar^2 n_k(t)}{m^* k_B T} \right] - 1 \right\},$$

which is measured from E_0. In Eq. (2), $v_k^d[\mathscr{E}_k(t)]$ is the drift velocity of electrons in the kth barrier layer, given by [1]

$$v_k^d[\mathscr{E}_k(t)] = \left[\frac{\mathscr{E}_k(t)}{\sqrt{\mathscr{E}_k^2(t) + \mathscr{E}_s^2}} \right] v_s$$

with the saturation velocity v_s and saturation field $\mathscr{E}_s$, respectively.

As explained in Fig. 1, the distribution of field domains changes with the value of the voltage $V_b(t)$ applied to the sample. When $V_b(t)$ varies with time, the charge density will fluctuate in each QW, accompanied by field domains that vary adiabatically across the whole sample. In this case, the charge-density fluctuation $\rho_j(t) = en_j(t)$ can be described by the equation [6]

$$\frac{d\rho_j(t)}{dt}$$

$$= P_c \sum_{k=1}^{j-1} (1 - P_c)^{j-k-1} J_k^{2D}[\mu_k(t), \mu_{k+1}(t), \mathscr{E}_k(t)] \theta[\mathscr{E}_k(t)]$$

$$+ P_c(1 - P_c)^{j-1} J_{inj}^{3D}[\mu_0, \mu_1(t), \mathscr{E}_0(t)] \theta[\mathscr{E}_0(t)]$$

$$- P_c \sum_{k=j+1}^{N} (1 - P_c)^{k-j-1} J_k^{2D}[\mu_k(t), \mu_{k-1}(t), \mathscr{E}_{k-1}(t)]$$

$$\times \theta[-\mathscr{E}_{k-1}(t)] - P_c(1 - P_c)^{N-j} J_{inj}^{3D}[\mu_0, \mu_N(t), \mathscr{E}_N(t)]$$

$$\times \theta[-\mathscr{E}_N(t)] - J_j^{2D}[\mu_j(t), \mu_{j+1}(t), \mathscr{E}_j(t)] \theta[\mathscr{E}_j(t)]$$

$$+ J_j^{2D}[\mu_j(t), \mu_{j-1}(t), \mathscr{E}_{j-1}(t)] \theta[-\mathscr{E}_{j-1}(t)], \tag{3}$$

where the small diffusion current [6,9] is neglected, $\theta(x)$ equals one for $x > 0$ and zero for $x \leqslant 0$, $j = 1, 2, \ldots, N$, and $0 \leqslant P_c \leqslant 1$ is the capture probability of electrons into the QW. The first two terms in Eq. (3) represent the forward contributions from capture current into the jth QW, while the third and fourth terms represent the backward contributions from capture current into that QW. The last two terms correspond to the forward and backward tunneling currents flowing out of the jth QW, respectively.

If electrons in QWs can be simply viewed as a distribution of sheet charges (zero-thickness), we get the following boundary conditions [6] from the Maxwell equations for two local fields on both sides the jth QW

$$\mathscr{E}_j(t) - \mathscr{E}_{j-1}(t) = \frac{1}{\epsilon_0 \epsilon_r}[\rho_j(t) - en_{2D}], \tag{4}$$

where quantum properties of an electron gas in a QW have been ignored, n_{2D} is the electron number density in equilibrium, $j = 1, 2, \ldots, N$ and ϵ_r is the relative dielectric constant of the well material. Finally, the sum of individual voltage drops on each period (well plus barrier) is fixed by the voltage $V_b(t)$. This restraint gives rise to

$$L_B \mathscr{E}_0(t) + (L_B + L_W) \sum_{k=1}^{N} \mathscr{E}_k(t) = V_b(t) \tag{5}$$

and $L_t = L_B + N(L_B + L_W)$ is the total length of the MQW structure in Fig. 1.

Combining Eqs. (3) and (4) for forward contributions we know that the sum of the displacement and conduction currents is a constant for $P_c = 1$, i.e.

$$\epsilon_0 \epsilon_r \frac{d\mathscr{E}_{j-1}(t)}{dt} + J_{j-1}^{2D}[\mu_{j-1}(t), \mu_j(t), \mathscr{E}_{j-1}(t)]$$

$$= \epsilon_0 \epsilon_r \frac{d\mathscr{E}_j(t)}{dt} + J_j^{2D}[\mu_j(t), \mu_{j+1}(t), \mathscr{E}_j(t)].$$

However, the conduction current itself is not a constant, which creates classical charge-density fluctuations and field domains in MQWs. For non-steady state, the initial condition for Eq. (3) can be set as $\rho_j(0) = en_{2D}$ if the ac electric field is applied to the sample after $t = 0$. Eqs. (3)–(5) together (totally $2N + 1$ equations) allow us to simultaneously solve for the charge-density distributions

$\rho_k(t)$ (or chemical-potential distributions $\mu_k(t)$) for $k = 1, 2, \ldots, N$, as well as for the local-field distributions $\mathscr{E}_k(t)$ for $k = 0, 1, 2, \ldots, N$ beyond steady state. For steady state with $d\rho_j(t)/dt = 0$, only forward contributions will stay. In this case, we only need to replace Eq. (3) at each moment by [8]

$$J_j^{2D}[\mu_j, \mu_{j+1}, \mathscr{E}_j] = P_c J_{inj}^{3D}[\mu_0, \mu_1, \mathscr{E}_0]$$

with $j = 1, 2, \ldots, N$. Under this condition, the measured tunneling current density simply equals $J_{inj}^{3D}[\mu_0, \mu_1, \mathscr{E}_0]$. But this does not imply a uniform distribution of charge densities and electric fields.

3. Quantum charge fluctuations

It has been known for a long time that a uniform-field distribution will underestimate or overestimate the sequential-tunneling current in MQWs at high or low voltages, respectively, [8] while the charge density will remain in its equilibrium value even when the uniform electric field is an ac field. In the classical field-domain model [6,8], quantum properties of electrons in QWs have been ignored. On the other hand, it has also been shown that the quantum non-adiabatic effects give rise to a residual current at zero of applied ac voltage due to a space-charge-field effect in the presence of a uniform ac electric field [2,5,11,12]. Therefore, it is very important to include, simultaneously, both the classical field-domain effect and the quantum non-adiabatic effect on the sequential tunneling of electrons in MQWs when an ac electric field is applied to the sample.

When the quantum non-adiabatic effect is included, Eq. (3) for $j = 1, 2, \ldots, N$ should be modified to

$$\begin{aligned}
\frac{d\rho_j(t)}{dt} &= P_c(1-P_c)^{j-1} J_{inj}^{3D}[\mu_0, \mu_1(t), \mathscr{E}_0(t)]\theta[\mathscr{E}_0(t)] \\
&\quad + P_c \sum_{k=1}^{j-1}(1-P_c)^{j-k-1} \\
&\quad \times J_k^{2D}[\mu_k(t) - eL_B\mathscr{E}_k^{na}(t), \mu_{k+1}(t), \mathscr{E}_k'(t)] \\
&\quad \times \theta[\mathscr{E}_k'(t)] - P_c(1-P_c)^{N-j}J_{inj}^{3D}[\mu_0, \mu_N(t), \mathscr{E}_N(t)]
\end{aligned}$$

$$\begin{aligned}
&\times \theta[-\mathscr{E}_N(t)] - P_c \sum_{k=j+1}^{N}(1-P_c)^{k-j-1} \\
&\times J_k^{2D}[\mu_k(t) - eL_B\mathscr{E}_k^{na}(t), \mu_{k-1}(t), \mathscr{E}_{k-1}'(t)] \\
&\times \theta[-\mathscr{E}_{k-1}'(t)] - J_j^{2D}[\mu_j(t) - eL_B\mathscr{E}_j^{na}(t), \mu_{j+1}(t), \mathscr{E}_j'(t)] \\
&\times \theta[\mathscr{E}_j'(t)] + J_j^{2D}[\mu_j(t) - eL_B\mathscr{E}_j^{na}(t), \mu_{j-1}(t), \mathscr{E}_{j-1}'(t)] \\
&\times \theta[-\mathscr{E}_{j-1}'(t)] - \frac{L_B}{\mathscr{S}}C_{QW}\frac{d\mathscr{E}_j^{na}(t)}{dt},
\end{aligned} \tag{6}$$

where the last term represents the non-adiabatic increase of charge density in the jth QW, $\mathscr{E}_j^{na}(t)$ is the non-adiabatic space-charge field in the jth QW and barrier, $\mathscr{S}$ is the cross-sectional area of the sample and $C_{QW} = (m^* e^2 \mathscr{S}/\pi\hbar^2)f_0[E_0 - \mu_e(n_{2D}, T)]$ is the quantum capacitance with chemical potential $\mu_e(n_{2D}, T)$ for an equilibrium two-dimensional electron gas in QWs. The non-adiabatic space-charge fields $\mathscr{E}_j^{na}(t)$ for $j = 1, 2, \ldots, N$ in Eq. (6) are determined by the following differential equations [5,11,12]

$$C_{QW}\frac{d\mathscr{E}_j^{na}(t)}{dt} = C_{QW}\frac{d\overline{\mathscr{E}}_j(t)}{dt} - \frac{\mathscr{S}}{L_B}\Delta J_j^{na}(t), \tag{7}$$

which contains a "quantum displacement" current due to C_{QW} as a source term. The non-adiabatic change of current density in Eq. (7) is

$$\begin{aligned}
\Delta J_j^{na}(t) &= J_j^{2D}[\mu_j(t) - eL_B\mathscr{E}_j^{na}(t), \mu_{j+1}(t), \mathscr{E}_j'(t)]\theta[\mathscr{E}_j'(t)] \\
&\quad - J_j^{2D}[\mu_j(t) - eL_B\mathscr{E}_j^{na}(t), \mu_{j-1}(t), \mathscr{E}_{j-1}'(t)]\theta[-\mathscr{E}_{j-1}'(t)] \\
&\quad - J_j^{2D}[\mu_j(t), \mu_{j+1}(t), \mathscr{E}_j(t)]\theta[\mathscr{E}_j(t)] \\
&\quad + J_j^{2D}[\mu_j(t), \mu_{j-1}(t), \mathscr{E}_{j-1}(t)]\theta[-\mathscr{E}_{j-1}(t)]
\end{aligned}$$

with $\mathscr{E}_{N+1}^{na}(t) = 0$. The charge-density fluctuations in Eq. (6) now contain both adiabatic and non-adiabatic contributions. The last term in Eq. (6) represents the non-adiabatic contributions. The total field $\mathscr{E}_k'(t)$ and the average field $\overline{\mathscr{E}}_j(t)$ in Eqs. (6) and (7) are defined by

$$\begin{bmatrix} \mathscr{E}_k'(t) \\ \overline{\mathscr{E}}_k(t) \end{bmatrix} = \begin{bmatrix} \mathscr{E}_k(t) + \mathscr{E}_k^{na}(t) \\ [\mathscr{E}_k(t) + \mathscr{E}_{k-1}(t)]/2 \end{bmatrix}.$$

Simultaneously, Eq. (4) should also be modified to

$$\begin{aligned}
&\mathscr{E}_j(t) - \mathscr{E}_{j-1}(t) - \frac{C_{QW}}{C_0}\mathscr{E}_j^{na}(t) \\
&= \frac{1}{\epsilon_0\epsilon_r}[\rho_j(t) - en_{2D}],
\end{aligned} \tag{8}$$

where $C_0 = \epsilon_0 \epsilon_r \mathscr{S}/L_B$ is the classical geometric capacitance. For non-steady state, the total measured current density for $V_b(t) \geqslant 0$ is given by

$$
\begin{aligned}
J_m^{ns(+)}&(t) \\
&= (1-P_c)^N J_{inj}^{3D}[\mu_0, \mu_1(t), \mathscr{E}_0(t)]\theta[\mathscr{E}_0(t)] \\
&\quad + \sum_{k=1}^{N} (1-P_c)^{N-k} J_k^{2D}[\mu_k(t) - eL_B\mathscr{E}_k^{na}(t), \mu_{k+1}(t), \mathscr{E}_k'(t)] \\
&\quad \times \theta[\mathscr{E}_k'(t)] + J_{inj}^{3D}[\mu_0, \mu_N(t), \mathscr{E}_N(t)]\theta[-\mathscr{E}_N(t)] \\
&\quad + \frac{L_B C_0}{\mathscr{S}} \frac{d\mathscr{E}_N(t)}{dt},
\end{aligned}
\tag{9}
$$

which includes both conduction and dielectric displacement currents, where the last term represents the displacement current from the geometric capacitance. In this case, the in-flowing injection current is not equal to the out-flowing conduction current from the sample due to $d\rho_j(t)/dt \neq 0$. On the other hand, for $V_b(t) < 0$ we have

$$
\begin{aligned}
J_m^{ns(-)}&(t) \\
&= (1-P_c)^N J_{inj}^{3D}[\mu_0, \mu_N(t), \mathscr{E}_N(t)]\theta[-\mathscr{E}_N(t)] \\
&\quad + \sum_{k=1}^{N} (1-P_c)^{k-1} \\
&\quad \times J_k^{2D}[\mu_k(t) - eL_B\mathscr{E}_{k-1}^{na}(t), \mu_{k-1}(t), \mathscr{E}_{k-1}'(t)] \\
&\quad \times \theta[-\mathscr{E}_{k-1}'(t)] + J_{inj}^{3D}[\mu_0, \mu_1(t), \mathscr{E}_0(t)]\theta[\mathscr{E}_0(t)] \\
&\quad + \frac{L_B C_0}{\mathscr{S}} \frac{d\mathscr{E}_0(t)}{dt}.
\end{aligned}
\tag{10}
$$

In steady state, however, there is no non-adiabatic charge-density fluctuation, and the total measured current density is mainly determined by the injection current, which is given for $V_b(t) \geqslant 0$ by

$$
J_m^s(t) = J_{inj}^{3D}[\mu_0, \mu_1(t), \mathscr{E}_0(t)] + \frac{L_B C_0}{\mathscr{S}} \frac{d\mathscr{E}_N(t)}{dt}, \tag{11}
$$

and can be modified by the local field at the emitter barrier. Moreover, due to $d\rho_j(t)/dt \neq 0$ in non-steady state we can define a total differential capacitance for the MQW structure

$$
C_{di}(t) \equiv \sum_{j=1}^{N} C_{di}^j(t) = \left[\frac{dV_b(t)}{dt}\right]^{-1} \mathscr{S} \sum_{j=1}^{N} \frac{d\rho_j(t)}{dt}, \tag{12}
$$

which is time-dependent and different from both C_0 and C_{QW}.

From Eq. (8) we know that both the field-domain and non-adiabatic effects will cause charge-density fluctuations in QWs in the presence of an ac electric field. The quantum capacitance C_{QW} only enters into Eq. (6) for the charge-density fluctuations but not into Eq. (9) for the total measured current density $J_m^{ns(\pm)}(t)$. Instead, the conduction current is modified by the non-adiabatic space-charge field $\mathscr{E}_j^{na}(t)$ which is induced by the "quantum displacement" current as shown in Eq. (7). On the other hand, the geometric capacitance C_0 directly modifies the total measured current in Eq. (9) as a contribution from the dielectric displacement current but does not enter into the charge fluctuations in Eq. (6). When only the forward contributions are included, the sum of dielectric displacement and conduction currents flowing into and out of a QW is a constant for $P_c = 1$. Because the conduction current flowing into the first QW is simply the injection current from the top contact layer, the change in the conduction currents flowing into different QWs is determined by the variation of the dielectric displacement currents due to the non-uniform electric-field distribution inside the whole system. From Eq. (7) we further find that even under a uniform ac electric field, the non-adiabatic conduction current density flowing through each QW is not equal to the sum of adiabatic sequential-tunneling current flowing out of the QW and the "quantum displacement" current density $L_B C_{QW} d\overline{\mathscr{E}}_j(t)/dt$ because $d\mathscr{E}_j^{na}(t)/dt \neq 0$.

4. Non-adiabatic self-consistent Hartree model

The non-equilibrium electron distribution function in a shifted Fermi–Dirac model [13] can be written as

$$
f^{\mu_0}(\mathbf{k}) = f_0^{\mu_0}(E_{|\mathbf{k}+\Delta\mathbf{k}|} + \Delta E_k), \tag{13}
$$

where $f_0^{\mu_0}(E_k)$ is defined by

$$
f_0^{\mu_0}(E_k) = \left\{1 + \exp\left[\frac{E_k - \mu_0(n_{2D}, T)}{k_B T}\right]\right\}^{-1}. \tag{14}
$$

For the shifted Fermi–Dirac model in Eq. (13), there exists a local charge-density fluctuation for each electron state $|\mathbf{k}\rangle$, defined by

$$\frac{d}{dt}\delta\rho_{\mathbf{k}}(t) = \frac{e}{\mathscr{V}}[f^{\mu_0}(\mathbf{k}) - f_0^{\mu_0}(E_k)]$$

$$= -\frac{e}{\mathscr{V}}\left\langle\frac{d\Delta E_k}{dt}\right\rangle_t\left[-\frac{\partial f_0^{\mu_0}(E_k)}{\partial E_k}\right], \qquad (15)$$

where $\mathscr{V}$ is the volume of the sample.

For a MQW system with thick barrier layers, the adiabatic sequential-tunneling current density flowing in the z direction (growth direction and perpendicular to the QW layers) is found to be

$$J^{\mu_0}(t)$$
$$= \frac{2e}{\mathscr{V}}\sum_{\mathbf{k}}v_k^z\mathscr{T}[E_k,|\mathscr{E}_{\mathrm{b}}|][f^{\mu_0}(E_k) - f^{\mu_0}(E_k + e|\mathscr{E}_{\mathrm{b}}|L_{\mathrm{B}})],$$
$$(16)$$

where v_k^z is the group velocity of electrons in the z direction, and $\mathscr{E}_{\mathrm{b}}$ stands for the applied electric field. If $\Omega\tau_{\mathrm{t}} \gg 1$ with τ_{t} being the electron sequential-tunneling time, $\mathscr{T}[E_k,|\mathscr{E}_{\mathrm{b}}|]$ has to be found by solving a time-dependent Schrödinger equation. Otherwise, $\mathscr{T}[E_k,|\mathscr{E}_{\mathrm{b}}|]$ can be calculated from a static Schrödinger equation at each time t if $\Omega\tau_{\mathrm{t}} \ll 1$. We will be only interested in the latter case with $\Omega\tau_{\mathrm{t}} \ll 1$ hereafter. If we replace $f^{\mu_0}(E_k)$ to leading-order approximation by the equilibrium value $f_0^{\mu_0}(E_k)$ in Eq. (14) for faster electron energy relaxation processes due to inelastic scattering of electrons compared to the electron sequential tunneling, and replace the electron group velocity v_k^z by a drift velocity $v_{\mathrm{d}}[\mathscr{E}_{\mathrm{b}}]$ (a statistically-averaged group velocity) of electrons in a bulk material, Eq. (16) reduces to Levine's sequential-tunneling model [1]

$$J^{\mu_0}[\mathscr{E}_{\mathrm{b}}] = \frac{2e}{\mathscr{V}}v_{\mathrm{d}}[\mathscr{E}_{\mathrm{b}}]\sum_{\mathbf{k}}\mathscr{T}[E_k,|\mathscr{E}_{\mathrm{b}}|][f_0^{\mu_0}(E_k)$$
$$- f_0^{\mu_0}(E_k + e|\mathscr{E}_{\mathrm{b}}|L_{\mathrm{B}})], \qquad (17)$$

where $v_{\mathrm{d}}[\mathscr{E}_{\mathrm{b}}] = (e\tau_{\mathrm{p}}/m^*)\mathscr{E}_{\mathrm{b}}$, and the momentum-relaxation time τ_{p} is given by

$$\tau_{\mathrm{p}} = \frac{m^*v_{\mathrm{s}}}{e\sqrt{\mathscr{E}_{\mathrm{s}}^2 + \mathscr{E}_{\mathrm{b}}^2}}. \qquad (18)$$

In Eq. (17), $J^{\mu_0}[\mathscr{E}_{\mathrm{b}}]/ev_{\mathrm{d}}[\mathscr{E}_{\mathrm{b}}]$ can be equivalently viewed as a three-dimensional tunneling-electron density which depends on $\mathscr{E}_{\mathrm{b}}$, T and n_{2D}.

From now on, we limit ourselves to an electrical-quantum limit where only the ground subband

of the quantum well is occupied by electrons at low temperatures and low electron densities. The electron kinetic energy of the ground subband (measured from the edge E_0) is given by $E_k = \hbar^2k^2/2m^*$. In the current-surge model [5,11,12], we assume that ΔE_k is associated with the global fluctuation (independent of individual electron state) of the chemical potential of electrons in the QW. By writing $\Delta E_k = -\Delta\mu = \mu_0(n_{\mathrm{2D}}, T) - \mu(t)$ for the global chemical-potential fluctuation, where $\mu(t)$ and $\mu_0(n_{\mathrm{2D}}, T)$ are, respectively, the transient chemical potential for electron density $n_{\mathrm{e}}(t)$ and that for an equilibrium electron gas in quantum wells, we get

$$\frac{d\Delta E_k}{dt} = \frac{\partial\Delta E_k}{\partial t} - \frac{\partial\mu}{\partial n_{\mathrm{e}}}\frac{dn_{\mathrm{e}}}{dt}. \qquad (19)$$

We further introduce a spatially-averaged non-adiabatic space-charge field $\mathscr{E}_{\mathrm{na}}(t)$ which is defined by [5,11,12]

$$\Delta E_k = e\mathscr{E}_{\mathrm{na}}(t)L_{\mathrm{B}}, \qquad (20)$$

where $\mathscr{E}_{\mathrm{na}}(t)$ measures the non-adiabatic reduction of the electron chemical potential in QWs under a uniform applied electric field. If we use Levine's sequential-tunneling model in Eq. (17), we find the following non-adiabatic current density due to the existence of this non-adiabatic space-charge field $\mathscr{E}_{\mathrm{na}}(t)$

$$\Delta J_{\mathrm{na}}(t) = J^{\mu_0 - eL_{\mathrm{B}}\mathscr{E}_{\mathrm{na}}}[\mathscr{E}_{\mathrm{b}} + \mathscr{E}_{\mathrm{na}}] - J^{\mu_0}[\mathscr{E}_{\mathrm{b}}], \qquad (21)$$

where $J^{\mu_0}[\mathscr{E}_{\mathrm{b}}]$ has been given in Eq. (17). In Eq. (21), the first term can be viewed as an equivalent capture current into the QW, while the second term can be regarded as a sequential-tunneling current flowing out of the QW.

For a QW, the electron density will be constant if the conduction currents flowing in and out of the well are equal. The variation of the charge density in the well is created by an imbalance in conduction currents. The charge-current conservation law requires

$$\mathscr{V}\frac{d}{dt}\delta\rho(t) \equiv \mathscr{V}\frac{d}{dt}\sum_{\mathbf{k}}\delta\rho_{\mathbf{k}}(t) = \mathscr{S}\Delta J_{\mathrm{na}}(t). \qquad (22)$$

The left-hand side of Eq. (22) represents the non-adiabatic charge increase inside the well, while the right-hand-side of the equation stands for the net

increase of charge due to non-adiabatic current flowing into the QW.

If $\Omega\tau_t \ll 1$, the ground-state electron wave function $\phi_1(z,t)$ inside the QW within the self-consistent Hartree model is determined by [14]

$$
\left[-\frac{\hbar^2}{2}\frac{d}{dz}\left(\frac{1}{m^*(z)}\frac{d}{dz}\right) - e\mathscr{E}_b(t)z + U_{QW}(z) \right.
$$
$$
\left. + \mathscr{V}_H(z,t) \right]\phi_1(z,t) = E_0(t)\phi_1(z,t), \tag{23}
$$

where $E_0(t)$ is the time-dependent ground-subband edge, the electron effective mass $m^*(z)$ is m_W in the well and m_B in the barrier, and $U_{QW}(z)$ is zero inside the well but V_0 outside the well. Within the adiabatic limit, we have $\mu(t) = \mu_0(n_{2D}, T)$, otherwise $\delta\rho(t) \neq 0$ for non-adiabatic cases. The Hartree potential $\mathscr{V}_H(z,t)$ in Eq. (23) can be found from the Poisson equation

$$
\frac{d}{dz}\left[\epsilon_r(z)\frac{d}{dz}\mathscr{V}_H(z,t)\right] = \frac{e^2}{\epsilon_0}[N_D(z) - n_e(z,t)], \tag{24}
$$

where donors are assumed completely ionized, and the relative dielectric constant $\epsilon_r(z)$ is ϵ_W in the well and ϵ_B in the barrier. $N_D(z)$ in Eq. (24) is the static profile of donor doping for the single quantum well, $n_e(z,t) = |\phi_1(z,t)|^2 n_e(t)$ is the density function, and

$$
n_e(t) = n_{2D} + \delta\rho(t) = n_{2D} + \rho_{2D}\int_0^{+\infty} dE\,\delta f(E,t), \tag{25}
$$

where $\rho_{2D} = (m_W/\pi\hbar^2)$ is the density of states for two-dimensional electrons in the QW, $\delta f(E,t)$ represents the local non-adiabatic fluctuation of the electron distribution function in energy space. Here, the number of electrons in the quantum well is not a constant due to the non-adiabatic current flowing. Moreover, we find from Eqs. (15), (19) and (25)

$$
\frac{d}{dt}\delta\rho(t)
$$
$$
= e\rho_{2D}\int_0^{+\infty} dE\,\frac{\partial}{\partial t}\delta f(E,t)
$$
$$
+ e^2 L_B\rho_{2D}\frac{d}{dt}\mathscr{E}_b(t)\int_0^{+\infty} dE\left[-\frac{\partial f_0^{\mu_0}(E)}{\partial E}\right]. \tag{26}
$$

Applying Eq. (22) and using Eqs. (21) and (26), we find the following integral equation for $\delta f(E,t)$ by using Levine's model in Eq. (17)

$$
e\rho_{2D}\int_0^{+\infty} dE\,\frac{\partial}{\partial t}\delta f(E,t)
$$
$$
+ e^2 L_B\rho_{2D}\frac{d\mathscr{E}_b(t)}{dt}\int_0^{+\infty} dE\left[-\frac{\partial f_0^{\mu_0}(E)}{\partial E}\right]
$$
$$
- \frac{e\rho_{2D}}{L_W}\{v_d[\mathscr{E}_b] + \delta v_d[\delta f]\}
$$
$$
\times \int_0^{+\infty} dE\,\mathscr{T}[E + E_0, |\mathscr{E}_b|; \mathscr{V}_H] \times [f_0^{\mu_0}(E)
$$
$$
+ \delta f(E,t) - f_0^{\mu_0}(E + e|\mathscr{E}_b|L_B) - \delta f(E + e|\mathscr{E}_b|L_B,t)]
$$
$$
+ \frac{e\rho_{2D}}{L_W}v_d[\mathscr{E}_b]\int_0^{+\infty} dE\,\mathscr{T}[E + E_0^{(0)}, |\mathscr{E}_b|; \mathscr{V}_H^{(0)}][f_0^{\mu_0}(E)
$$
$$
- f_0^{\mu_0}(E + e|\mathscr{E}_b|L_B)] = 0, \tag{27}
$$

where $\mathscr{T}[E + E_0, |\mathscr{E}_b|; \mathscr{V}_H]$ is the quantum transmission of electrons and can be calculated by iteration (see Appendix A). In Eq. (27), $\mathscr{V}_H(z,t)$ and $E_0(t)$ are written simply as $\mathscr{V}_H$ and E_0. The adiabatic quantities $\mathscr{V}_H^{(0)}(z,t)$ and $E_0^{(0)}(t)$ can be obtained by simply setting $\delta\rho(t) = 0$ in Eq. (24) and $\mathscr{V}_H(z,t) = \mathscr{V}_H^{(0)}(z,t)$ in Eq. (23). Moreover, $\delta v_d[\delta f]$ introduced in Eq. (27) is calculated to be

$$
\delta v_d[\delta f] = -\frac{\rho_{2D}}{2n_{2D}}\int_0^{+\infty} dE\,\delta f(E,t)\sqrt{\frac{2E}{m_W}}. \tag{28}
$$

Finally, Eq. (27) leads us to the non-adiabatic dynamical differential equation for $\delta f(E,t)$

$$
\frac{\partial}{\partial t}\delta f(E,t) - eL_B\frac{d\mathscr{E}_b(t)}{dt}\frac{\partial f_0^{\mu_0}(E)}{\partial E}
$$
$$
- \frac{1}{L_W}\{v_d[\mathscr{E}_b] + \delta v_d[\delta f]\}\mathscr{T}[E + E_0, |\mathscr{E}_b|; \mathscr{V}_H] \times [f_0^{\mu_0}(E)
$$
$$
+ \delta f(E,t) - f_0^{\mu_0}(E + e|\mathscr{E}_b|L_B) - \delta f(E + e|\mathscr{E}_b|L_B,t)]
$$
$$
+ \frac{1}{L_W}v_d[\mathscr{E}_b]\mathscr{T}[E + E_0^{(0)}, |\mathscr{E}_b|; \mathscr{V}_H^{(0)}][f_0^{\mu_0}(E)
$$
$$
- f_0^{\mu_0}(E + e|\mathscr{E}_b|L_B)] = 0, \tag{29}
$$

where the initial condition is chosen to be $\delta f(E,t) = 0$ at $t = 0$ if the ac electric field is applied to the system after $t = 0$. $\delta f(E,t)$ has a lower bound which is determined by the condition $\delta f(E,t) + f_0^{\mu_0}(E) = 0$.

For small $\Delta\mu$, the first term in Eq. (29) can be approximated to leading order by

$$\frac{\partial}{\partial t}\delta f(E,t) \approx \frac{\partial \Delta\mu}{\partial t}\left[-\frac{\partial f_0^{\mu_0}(E)}{\partial E}\right]. \tag{30}$$

Similarly, the third term in Eq. (29) can be approximated as

$$\mathscr{T}[E+E_0,|\mathscr{E}_b|;\mathscr{V}_H][f_0^{\mu_0}(E)+\delta f(E,t)$$
$$-f_0^{\mu_0}(E+e|\mathscr{E}_b|L_B)-\delta f(E+e|\mathscr{E}_b|L_B,t)]$$
$$\approx \mathscr{T}[E+E_0^{(0)},|\mathscr{E}_b|;\mathscr{V}_H^{(0)}+(\delta\mathscr{V}_H^{(0)}/\delta n_{2D})\rho_{2D}\Delta\mu]$$
$$\times [f_0^{\mu_0+\Delta\mu}(E)-f_0^{\mu_0+\Delta\mu}(E+e|\mathscr{E}_b|L_B)], \tag{31}$$

where $(\delta\mathscr{V}_H^{(0)}/\delta n_{2D})=(e^2/2\epsilon_0\epsilon_W q_{TF})$ and $q_{TF}=(e^2/2\epsilon_0\epsilon_W)\rho_{2D}$ from the Thomas–Fermi model [14]. By recalling $\Delta\mu=-e\mathscr{E}_{na}(t)L_B$, Eq. (29) results in the current-surge model [11], where

$$C_{QW}=e^2\mathscr{S}\rho_{2D}\int_0^{+\infty}dE\left[-\frac{\partial f_0^{\mu_0}(E)}{\partial E}\right],$$

$$J^{\mu_0}[\mathscr{E}_b]$$
$$=\frac{e\rho_{2D}}{L_W}v_d[\mathscr{E}_b]\int_0^{+\infty}dE\,\mathscr{T}\left[E+E_0^{(0)},|\mathscr{E}_b|;\mathscr{V}_H^{(0)}\right]$$
$$\times [f_0^{\mu_0}(E)-f_0^{\mu_0}(E+e|\mathscr{E}_b|L_B)],$$

$$\mathscr{T}\left[E+E_0^{(0)},|\mathscr{E}_b|;\mathscr{V}_H^{(0)}-e\mathscr{E}_{na}L_B\right]$$
$$\approx \mathscr{T}\left[E+E_0^{(0)},|\mathscr{E}_b+\mathscr{E}_{na}|;\mathscr{V}_H^{(0)}\right],$$

and $v_d[\mathscr{E}_b]+\delta v_d[\delta f]\approx v_d[\mathscr{E}_b+\mathscr{E}_{na}]$ if we set $\tau_p\approx L_B/v_F$ with v_F being the electron group velocity at the Fermi energy. The non-adiabatic space-charge field $\mathscr{E}_{na}(t)$ introduced by $\Delta\mu=-e\mathscr{E}_{na}(t)L_B$ can be calculated from

$$\mathscr{E}_{na}(t)=-\frac{1}{eL_B}\int_0^{+\infty}dE\,\delta f(E,t), \tag{32}$$

which becomes positive if $\delta\rho(t)<0$.

5. Numerical results

In this section, we first present numerical results for distributions of both local fields and charge densities in the presence of an applied ac electric field, including effects of classical and quantum charge fluctuations. After this, we present results for fluctuating electron distributions and Hartree potentials. The voltage is defined to be $V_b(t)=$ $\mathscr{E}_b(t)L_t$ with $\mathscr{E}_b(t)=\mathscr{E}_{dc}+\mathscr{E}_{ac}(t)$ and $\mathscr{E}_{ac}(t)=$ $\mathscr{E}_m\sin(2\pi t/T_p)$ for $t\geqslant 0$.

The sample 1 we consider for showing domain effects is an AlGaAs/GaAs MQW structure. The total number of QWs is $N=10$, with eleven barriers. The parameters for sample 1 are: well thickness $L_W=75$ Å, barrier thickness $L_B=339$ Å, barrier height $V_0=224.5$ meV, electron effective mass $m^*=0.065m_0$ with free electron mass m_0, electron areal density $n_{2D}=5\times10^{11}$ cm^{-2}, contact-layer electron concentration $n_c=6\times10^{17}$ cm^{-3}, cross-sectional area $\mathscr{S}=10^{-4}$ cm^2, capture probability $P_c=0.5$, saturation velocity $v_s=2\times10^6$ cm/s, saturation field $\mathscr{E}_s=2$ kV/cm, and relative dielectric constant $\epsilon_r=12$. For this sample, the ground-state subband edge is calculated to be $E_0=44.1$ meV. For the applied ac electric field, $\mathscr{E}_m=5$ kV/cm, $\mathscr{E}_{dc}=0$ and $T_p=0.1$ s. The sample 2 we chose for the non-adiabatic self-consistent Hartree model is also an AlGaAs/GaAs MQW structure. The parameters for sample 2 are: $L_W=80$ Å, $L_B=300$ Å, $V_0=331$ meV, electron effective mass in well $m_W=0.067m_0$, electron effective mass in barrier $m_W=0.092m_0$, $n_{2D}=4\times10^{11}$ cm^{-2}, $\mathscr{S}=2.25\times10^{-4}$ cm^2, $v_s=2\times10^6$ cm/s, $\mathscr{E}_s=2$ kV/cm, dielectric constant in well $\epsilon_W=12.0$, and dielectric constant in barrier $\epsilon_W=11.2$. $E_0^{(0)}$ is calculated to be 44.5 meV. For the applied electric field, $\mathscr{E}_{dc}=0.05$ kV/cm and $T_p=4$ s.

We show in Fig. 2 the local fields $\mathscr{E}_j(t)-\mathscr{E}_b(t)$ in different layers of sample 1 (in (a)) and the density fluctuation $n_j(t)-n_{2D}$ in different QW's (in (b)) at several times t/T_p for $T=77$ K. From (a) we find that the field-domain effect is negligible at $t/T_p=0.05$ (very small applied field) because both the injection current J_{inj}^{3D} and the sequential-tunneling current J_k^{2D} are both extremely small in this case. With the increase of $\mathscr{E}_b(t)$, i.e. t/T_p increases from 0.05 to 0.25, fields close to the emitter barrier are enhanced dramatically relative to the uniform field $\mathscr{E}_b(t)$. This is a result of the huge current imbalance $J_{inj}^{3D}\ll J_1^{2D}$ under the uniform field $\mathscr{E}_b(t)$, as explained in Fig. 1(b). At the same time, fields close to the receiver barrier are suppressed almost to zero. From (b) we find that when $\mathscr{E}_b(t)$ is large, densities close to the emitter barrier are greatly reduced with respect to the equilibrium
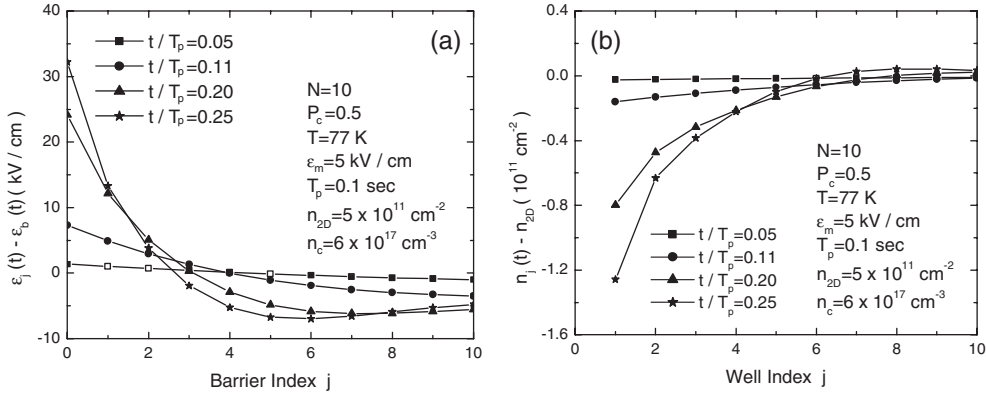
Fig. 2. Calculated local fields $\mathscr{E}_j(t) - \mathscr{E}_b(t)$ in (a) in different barrier layers and density fluctuations $n_j(t) - n_{2D}$ in (b) inside different QWs of sample 1 at times $t/T_p = 0.05, 0.11, 0.20$ and 0.25 s. The parameters used in calculations are given in the text.

value n_{2D}. This is accompanied by a great enhancement of the local field $\mathscr{E}_0(t) \gg \mathscr{E}_b(t)$ at the emitter barrier, as shown in (a). However, densities close to the receiver barrier remain near n_{2D} due to the suppressed local field $\mathscr{E}_N(t) \approx 0$. It is obvious from (b) that some electrons have been removed from the sample since $\sum_j [n_j(t) - n_{2D}] < 0$, which is true even for steady state. The calculation done here corresponds to a non-steady state. Therefore, the net number of electrons removed from the sample changes with time under an ac voltage, leading to a differential capacitance $C_{di}^j(t)$ (see Eq. (12)).

Fig. 3 compares local fields $\mathscr{E}_j(t) - \mathscr{E}_b(t)$ in sample 1 at $t/T_p = 0.25$ as a function of barrier index j for different values of $\mathscr{E}_m$, T_p, T in (a) and different values of N, n_{2D}, n_c in (b). From (a) we find that the field-domain effect is negligible at $T \leqslant 65$ K due to very small injection and sequential-tunneling currents at these temperatures. The bigger the field amplitude $\mathscr{E}_m$ is, the larger $\mathscr{E}_0(t)$ will be. A smaller T_p leads to a negative $\mathscr{E}_N(t)$ on the receiver barrier due to the strong non-steady effect. This is completely different from the steady-state results [8] in which $\mathscr{E}_N(t)$ will always be positive. Furthermore, we find from (b) that the
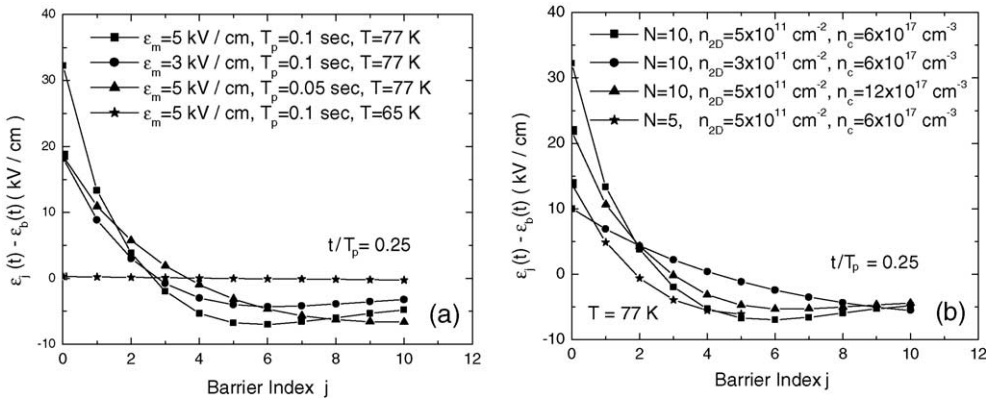

Fig. 3. Calculated local fields $\mathscr{E}_j(t) - \mathscr{E}_b(t)$ in different barrier layers of sample 1 at the time $t/T_p = 0.25$ s. Here, the comparison of $\mathscr{E}_j(t) - \mathscr{E}_b(t)$ with different values of $\mathscr{E}_m$, T_p and T are presented in (a) and the comparison of those with different values of N, n_{2D} and n_c are shown in (b). The changed parameters are indicated in figures. The other parameters used in calculations are the same as those in Fig. 2.
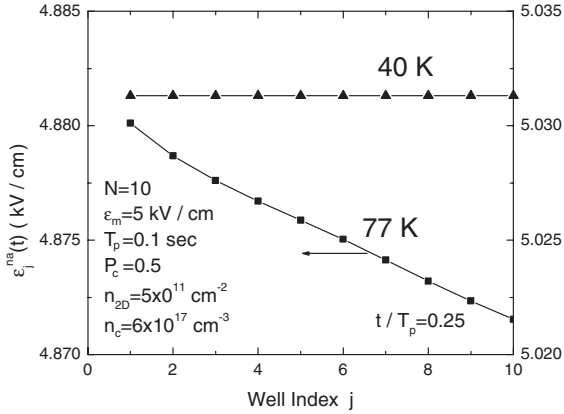
Fig. 4. Calculated non-adiabatic space-charge fields $\mathscr{E}_j^{\mathrm{na}}(t)$ in sample 1 at $t/T_{\mathrm{p}} = 0.25$ as a function of well index j for $T = 40$ and 77 K (left scaled), respectively. The other parameters used in calculations are the same as those in Fig. 2.

smaller the number of QW's N is, the lower $\mathscr{E}_0(t)$ is. The increase of $n_{2\mathrm{D}}$ causes a larger sequential-tunneling current, leading to a larger value of $\mathscr{E}_0(t)$ due to an enhanced current imbalance between $J_{\mathrm{inj}}^{3\mathrm{D}}$ and $J_1^{2\mathrm{D}}$. Conversely, the increase of n_{c} introduces a bigger injection current, leading to a smaller value of $\mathscr{E}_0(t)$ due to a suppressed current imbalance between $J_{\mathrm{inj}}^{3\mathrm{D}}$ and $J_1^{2\mathrm{D}}$.

Effects of classical charge fluctuations depend on the geometric capacitance C_0, as shown by Eq.

(4). However, the quantum capacitance C_{QW} starts to play a role when the non-adiabatic effect is included, as seen from Eq. (8). The striking thing is that the effects of quantum charge fluctuations become more and more important as $T \leqslant 65$ K, while the effects of classical charge fluctuations are negligible at these temperatures. We compare in Fig. 4 two calculated non-adiabatic fields $\mathscr{E}_j^{\mathrm{na}}(t)$ at $t/T_{\mathrm{p}} = 0.25$ in sample 1 as a function of well index j for $T = 40$ and 77 K. From the figure we know that $\mathscr{E}_j^{\mathrm{na}}(t)$ decreases with j due to field-domain effects at $T = 77$ K. However, $\mathscr{E}_j^{\mathrm{na}}(t)$ becomes independent of j at $T = 40$ K. More importantly, $\mathscr{E}_j^{\mathrm{na}}(t)$ increases with reducing T.

The effect of non-adiabatic field $\mathscr{E}_j^{\mathrm{na}}(t)$ can be seen more clearly from the calculated local fields $\mathscr{E}_j(t) - \mathscr{E}_{\mathrm{b}}(t)$ in different barrier layers of sample 1 in Fig. 5(a) and density fluctuations $n_j(t) - n_{2\mathrm{D}}$ in different QW's in Fig. 5(b) at $t/T_{\mathrm{p}} = 0.25$ with various values of $\mathscr{E}_{\mathrm{m}}$, T_{p} and T. By comparing solid and dashed curves in (a) we find that $\mathscr{E}_0(t)$ is reduced by a factor of 2 as $\mathscr{E}_{\mathrm{m}} = 5$ kV/cm, $T_{\mathrm{p}} = 0.1$ s and $T = 77$ K (squares). Moreover, $\mathscr{E}_0(t)$ decreases even more due to $\mathscr{E}_j^{\mathrm{na}}(t)$ when T_{p} is reduced to 0.05 s (stars) due to stronger non-steady effects, but it decreases much less when T is reduced to 40 K (triangles) due to smaller injection and sequential-tunneling currents. However, $\mathscr{E}_0(t)$ is enhanced by non-adiabatic effects when $\mathscr{E}_{\mathrm{m}}$ is reduced to
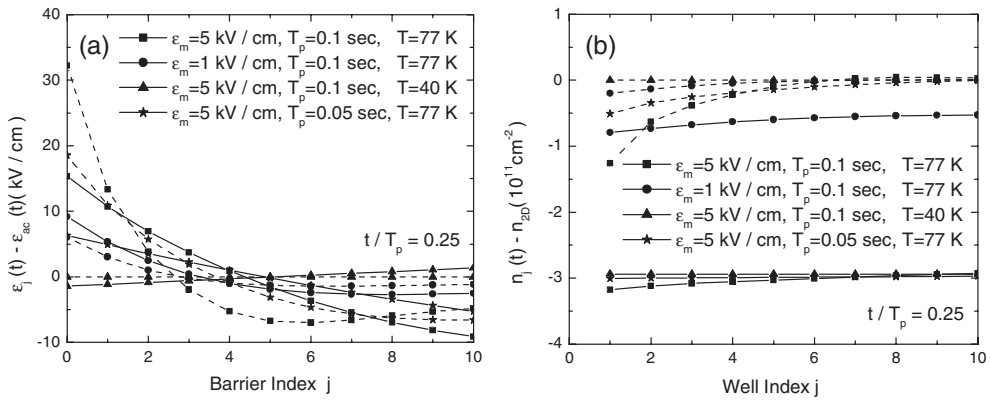

Fig. 5. Calculated local fields $\mathscr{E}_j(t) - \mathscr{E}_{\mathrm{b}}(t)$ in different barrier layers of sample 1 and density fluctuations $n_j(t) - n_{2\mathrm{D}}$ inside different QWs at $t/T_{\mathrm{p}} = 0.25$ with different values of $\mathscr{E}_{\mathrm{m}}$ (squares and circles), T_{p} (squares and stars) and T (squares and triangles). $\mathscr{E}_j(t) - \mathscr{E}_{\mathrm{b}}(t)$ are compared in (a) with (solid curves) and without (dashed curves) $\mathscr{E}_j^{\mathrm{na}}(t)$, and the similar comparisons of $n_j(t) - n_{2\mathrm{D}}$ are presented in (b). The changed parameters are indicated in figures. The other parameters used in calculations are the same as those in Fig. 2.

1 kV/cm (circles). On the other hand, from (a) we also find that $\mathscr{E}_N(t)$ becomes a much more negative value for $\mathscr{E}_m = 5$ kV/cm, $T_p = 0.1$ s and $T = 77$ K when $\mathscr{E}_j^{na}(t)$ is included in our calculations (solid curve with squares) than when it is excluded (dashed curve with squares). The same situation occurs when either T_p is reduced to 0.05 s (stars) or $\mathscr{E}_m$ is reduced to 1 kV/cm (circles) but with a smaller overall magnitude compared to the curves with the squares. The features observed for $\mathscr{E}_N(t)$ in Fig. 5(a) will affect the conduction current detected at the receiver layer. Effects of quantum charge fluctuations are reflected in the calculated $n_j(t) - n_{2D}$ in (b), where the reduction of charge in the QWs is greatly increased except for the case with small value of $\mathscr{E}_m$ (circles). Although there is a strong dependence of $\mathscr{E}_j(t)$ on index j near the emitter barrier, there is very little dependence of $n_j(t)$ on j there after $\mathscr{E}_j^{na}(t)$ is included in the calculations.

In order to gain further information about the local change in the non-adiabatic electron distribution function, we display $\delta f(E,t)$ of sample 2 in Fig. 6 at $t/T_p = 0.25$ with uniform doping for different values of T. From the figure it is clear that $\delta f(E,t)$ always shows a negative minimum at $\mu_0(n_{2D}, T)$ since it is proportional to $\partial f_0^{\mu_0}(E)/\partial E$. Since the Fermi surface broadens with increasing T, we find from the figure that the negative minimum is partially suppressed and broadened (solid curve) when $T = 40$ K compared to that at
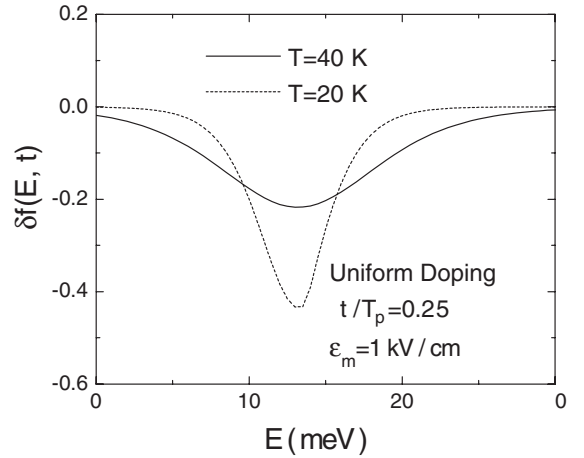

Fig. 6. Calculated non-adiabatic change in distribution functions $\delta f(E,t)$ at $t/T_p = 0.25$ for electrons in sample 2 with uniformly doped QWs. In this figure, we set $\mathscr{E}_m = 1$ kV/cm with $T = 40$ K (solid curve) and $T = 20$ K (dashed curve).

$T = 20$ K. We also find that the negative minimum is enhanced when $\mathscr{E}_m$ is increased (not shown).

Fig. 7(a) and (b) present non-adiabatic charging effects in the uniformly-doped QW on the Hartree potentials for sample 2 at $T = 40$ K and $\mathscr{E}_m = 1$ kV/cm. From (a) we find that the positive peak in the adiabatic Hartree potential $V_H^{(0)}(z,t)$ at the center of the QW is greatly suppressed by the non-adiabatic effect at $t/T_p = 0.25$, leaving two positive spikes at the edges of the QW. Fig. 7(b) shows the comparison between non-adiabatic Hartree po-
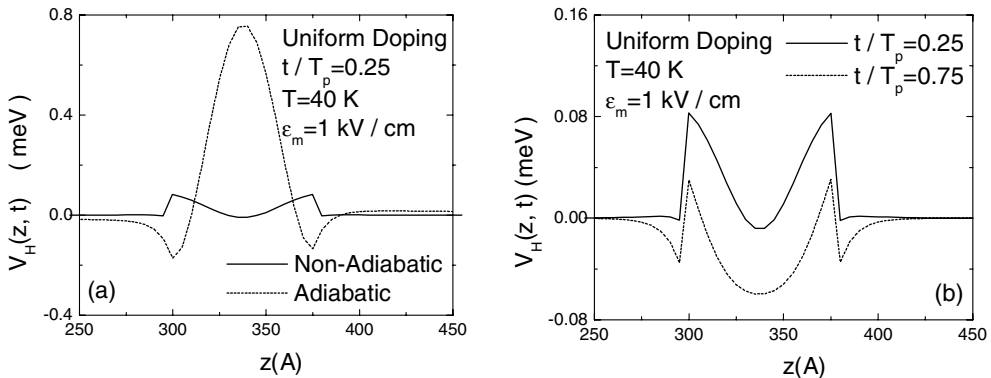

Fig. 7. Calculated position z dependence of non-adiabatic (solid curve) and adiabatic (dashed curve) Hartree potentials of sample 2 in (a) at $T = 40$ K and $\mathscr{E}_m = 1$ kV/cm with uniform doping inside the QW and non-adiabatic Hartree potentials $V_H(z,t)$ in (b) for $t/T_p = 0.25$ (solid curve) and $t/T_p = 0.75$ (dashed curve).
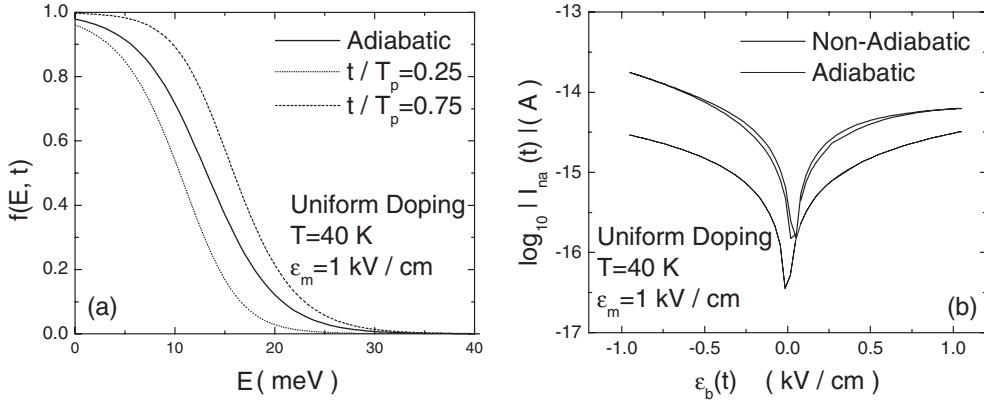
Fig. 8. Calculated non-adiabatic electron distribution functions $f(E, t)$ in (a) and logarithm of absolute value of total non-adiabatic sequential-tunneling current $I_{na}(t) = \mathscr{S}[J^{\mu_0}[\mathscr{E}_b] + \Delta J_{na}(t)]$ of sample 2 as a function of applied ac electric field $\mathscr{E}_b(t)$ in (b) for $T = 40$ K and $\mathscr{E}_m = 1$ kV/cm. In (a), we plot $f(E, t)$ at $t/T_p = 0.25$ (dotted curve) and $t/T_p = 0.75$ (dashed curve). The time-independent adiabatic electron distribution function $f_0^{\mu_0}(E)$ (solid curve) is also shown for the comparison. In (b), the currents calculated from adiabatic (lower curve) and non-adiabatic (upper curve) electron sequential tunneling are compared with each other.

tentials when electrons in the QW are either removed ($t/T_p = 0.25$, solid curve) or added ($t/T_p = 0.75$, dashed curve). We find from (b) that the two positive spikes at the edges of the QW are suppressed but two negative spikes are enhanced when electrons are added to the well.

Finally, we display in Fig. 8 $f(E, t)$ of sample 2 at $t/T_p = 0.25$ (dotted curve) and 0.75 (dashed curve), as well as in the adiabatic approximation, ($f_0^{\mu_0}(E)$, solid curve) in (a) and the $\log_{10} |I_{na}(t)|$ as a function of $\mathscr{E}_b(t)$ in (b). From (a) we see $f(E, t)$ has a fluctuation in time with respect to the adiabatic $f_0^{\mu_0}(E)$ around the Fermi energy. Compared with the adiabatic electron sequential-tunneling current (lower solid curve with $\Delta J_{na}(t) = 0$) in (b), the symmetry of $\log_{10} |I_{na}(t)|$ with respect to the positive (electrons being removed) and negative (electrons being added) peaks of $\mathscr{E}_b(t)$ is broken in the non-adiabatic case (upper solid curve). A small offset [5] of the non-adiabatic $\log_{10} |I_{na}(t)|$ relative to $\mathscr{E}_b(t) = 0$ can be seen by comparing upper and lower solid curves.

6. Conclusions

In conclusion, by including non-adiabatic space-charge-field effects we have generalized the previous theories for studying field-domain effects

in MQW photodetectors in the presence of an ac voltage. We have found from our numerical calculations that field-domain effects are only important at high temperatures or high voltages, which implies the existence of significant injection and sequential-tunneling currents in the system. We have further found that non-adiabatic effects become much more visible at low temperatures and low voltages when the field-domain effects are negligible. Furthermore, we have derived a dynamical differential equation for the non-adiabatic electron distribution function for sequential-tunneling current flowing through a MQW system. Using this equation, we generalized the self-consistent Hartree model for the calculation of non-adiabatic electronic states in a quantum well. Finally, we have connected the current quantum-statistical theory to the previously-proposed current-surge model with a leading-order approximation.

In this paper, we have assumed the capture probability is independent of electric field. This can be justified by the fact that the capture probability is nearly constant at low electric fields. In the presence of incident photons, the conduction current flowing through the MQW sample will be the sum of sequential-tunneling and photoexcited currents. From our studies in this paper, we predict that the field-domain effects which are significant at

high temperatures or high photon fluxes will strongly affect both tunneling- and photocurrents. On the other hand, non-adiabatic effects modify these currents at low temperatures and low photon fluxes when the current flowing through the MQWs is small. These latter conditions are of utmost importance in any space-based detector applications. Furthermore, only the self-consistent Hartree model is employed. The exchange interaction between electrons is expected to be very small [16] at $T = 40$ K and has been neglected.

The time scale for observing the non-adiabatic space-charge effect requires

$$t < R_{\mathrm{t}} C_{\mathrm{QW}} \mathscr{S} \ll \tau_{\mathrm{t}} \ll 2\pi/\Omega,$$

where $R_{\mathrm{t}} = (L_{\mathrm{B}}/\mathscr{S})[\partial J^{\mu_0}[\mathscr{E}_{\mathrm{b}}]/\partial \mathscr{E}_{\mathrm{b}}]^{-1}$ is the differential tunneling resistance, depending on $\mathscr{E}_{\mathrm{b}}$ and T. Further, $\Omega \tau_{\mathrm{t}} \ll 1$ ensures the electrons see only an instantaneous ac electric field during the sequential-tunneling process. Finally, $t < R_{\mathrm{t}} C_{\mathrm{QW}} \mathscr{A}$ ensures the observation of a non-adiabatic space-charge effect inside the QW. The tunneling time τ_{t} can be estimated from $\tau_{\mathrm{t}} \sim e/[J^{\mu_0}[\mathscr{E}_{\mathrm{b}}]\mathscr{S}]$. For a superlattice, we take $J^{\mu_0}[\mathscr{E}_{\mathrm{b}}]\mathscr{A} = 1$ μA, leading to $\tau_{\mathrm{t}} = 0.1$ ps and $\Omega \ll 10^{13}$ Hz from $\Omega \tau_{\mathrm{t}} \ll 1$. For a MQW system, we take $J^{\mu_0}[\mathscr{E}_{\mathrm{b}}]\mathscr{S} = 10$ pA, leading to $\tau_{\mathrm{t}} = 10$ ns and $\Omega \ll 10^8$ Hz. Difficulties in observing the non-adiabatic effect may come from the small QW capacitance $C_{\mathrm{QW}} \mathscr{S} \sim 100$ pF in the requirement $t < R_{\mathrm{t}} C_{\mathrm{QW}} \mathscr{S}$. For a superlattice, we take $R_{\mathrm{t}} = 10^4$ Ω, and then $t < 10^{-6}$ s is required (very hard to observe). For a MQW system, on the other hand, we take $R_{\mathrm{t}} = 10^{11}$ Ω, which implies $t < 10$ s (very easy to observe).

Acknowledgements

Appendix A

The quantum-mechanical transmission coefficient $\mathscr{T}[E + E_1, \mathscr{E}_{\mathrm{b}}; \mathscr{V}_{\mathrm{H}}]$ used to evaluate the tunneling current in Eq. (27) can be found from the following backward iteration [15] at each time t

$$\phi_{j-1}(t) = \left\{ 2 + \frac{1}{E_{\mathrm{d}}} \left[U_j^{\mathrm{B}} - e\mathscr{E}_{\mathrm{b}}(t)(j-1)\varDelta \right. \right.$$
$$\left. \left. + V_j^{\mathrm{H}}(t) - E - E_1(t) \right] \right\} \phi_j(t) - \phi_{j+1}(t)$$
$$(\mathrm{A.1})$$

for $1 \leqslant j \leqslant N_{\mathrm{B}}$, where $\phi_j(t) = \phi_1(z_j, t)$, $V_j^{\mathrm{H}}(t) = V_{\mathrm{H}}(z_j, t)$, $E_{\mathrm{d}} = \hbar^2/2m_{\mathrm{B}}\varDelta^2$, $\varDelta = L_{\mathrm{B}}/N_{\mathrm{B}}$ and N_{B} is the number of slabs (thickness $\varDelta$) within the barrier layer. Here, $U_j^{\mathrm{B}} = 0$ for $j = 0$ and $j = N_{\mathrm{B}} + 1$. Otherwise, $U_j^{\mathrm{B}} = V_0$. The ending boundary condition of Eq. (A.1) produces

$$\begin{bmatrix} \phi_{N_{\mathrm{B}}+1}(t) \\ \phi_{N_{\mathrm{B}}}(t) \end{bmatrix} = \begin{bmatrix} \exp(\mathrm{i}N_{\mathrm{B}}\bar{k}') \\ \{1 - \mathrm{i}\bar{k}' - (1/2E_{\mathrm{d}})[E + E_1(t) - U_{N_{\mathrm{B}}+1}^{\mathrm{B}} + e\mathscr{E}_{\mathrm{b}}(t)N_{\mathrm{B}}\varDelta - V_{N_{\mathrm{B}}+1}^{\mathrm{H}}(t)]\}\phi_{N_{\mathrm{B}}+1}(t) \end{bmatrix}, \quad (\mathrm{A.2})$$

where $\bar{k}' = (\varDelta/\hbar)\sqrt{2m_{\mathrm{B}}(E + e\mathscr{E}_{\mathrm{b}}(t)L_{\mathrm{B}})}$. From the solution of Eq. (A.1) we find the quantum-mechanical transmission of electrons from

$$\mathscr{T}[E + E_1, \mathscr{E}_{\mathrm{b}}; \mathscr{V}_{\mathrm{H}}] = \frac{1}{|S|^2}\sqrt{\frac{E + e\mathscr{E}_{\mathrm{b}}(t)L_{\mathrm{B}}}{E}}, \quad (\mathrm{A.3})$$

where $|S|^2 = [|a|^2 + |b|^2 + 2\mathrm{Re}(ab^*)]/4$. Here, the two complex numbers, a and b, are defined by the starting boundary condition of Eq. (A.1)

$$\begin{bmatrix} a \\ b \end{bmatrix} = \begin{bmatrix} \phi_1(t) \\ -(\mathrm{i}/2\bar{k})(\phi_2(t) - \phi_0(t)) \end{bmatrix} \quad (\mathrm{A.4})$$

with $\bar{k} = (\varDelta/\hbar)\sqrt{2m_{\mathrm{B}}E}$.

References

[1] B.F. Levine, J. Appl. Phys. 74 (1993) R1.
[2] A. Singh, D.A. Cardimona, Opt. Eng. 38 (1999) 1424.
[3] J.E. Hubbs, D.C. Arrington, M.E. Grammer, G.A. Dole, Opt. Eng. 39 (2000) 2660.

[4] K.K. Choi, S.W. Kennerly, J. Yao, D.C. Tsui, Infrared Phys. Technol. 42 (2001) 221.

[5] D.H. Huang, C. Morath, D.A. Cardimona, A. Singh, J. Appl. Phys. 90 (2001) 6032.

[6] M. Ershov, V. Ryzhii, C. Hamaguchi, Appl. Phys. Lett. 67 (1995) 3147.

[7] A.L. Fetter, J.D. Walecka, Quantum Theory of Many-Particle Systems, McGraw-Hill, New York, 1971 (Chapter 8).

[8] L. Thibaudeau, P. Bois, J.Y. Duboz, J. Appl. Phys. 79 (1996) 446.

[9] R. Aguado, G. Platero, M. Moscoso, L. Bonilla, Phys. Rev. B 55 (1997) R16053.

[10] D.H. Huang, A. Singh, D.A. Cardimona, Phys. Lett. A 259 (1999) 488.

[11] D.H. Huang, A. Singh, D.A. Cardimona, J. Appl. Phys. 87 (2000) 2427.

[12] D.H. Huang, A. Singh, D.A. Cardimona, C. Morath, J. Appl. Phys. 89 (2001) 4429.

[13] K. Flensberg, T.S. Jensen, N.A. Mortensen, Phys. Rev. B 64 (2001) 245308.

[14] D.H. Huang, Phys. Rev. B 53 (1996) 13645.

[15] D.H. Huang, D.A. Cardimona, A. Singh, Phys. Lett. A 243 (1998) 335.

[16] D.H. Huang, G. Gumbs, M.O. Manasreh, Phys. Rev. B 52 (1995) 14126.